ChemComm

Accepted Manuscript

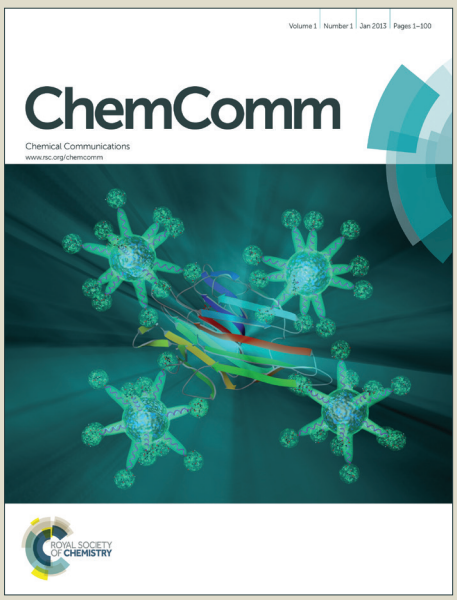

ROYAL SOCIETY OF CHEMISTRY

www.rsc.org/chemcomm

Journal Name

RSCPublishing

COMMUNICATION

Catalyst free silica templated porous carbon nanoparticles from bio-waste materials

Cite this: DOI: 10.1039/x0xx00000x

A. Kumar,[a,b] G. Hegde[*a], S. A. Abdul Manaf [a], Z. Ngaini[c] and K.V. Sharma[d]

Received 00th January 2012,
Accepted 00th January 2012

DOI: 10.1039/x0xx00000x

www.rsc.org/

Porous Carbon Nanoparticles (PCNs) with well-developed microporosity were obtained from bio-waste oil palm leaves (OPL) using single step pyrolysis in nitrogen atmosphere at 500–600 ^{o}C in tube-furnace without any catalysis support. The key approach was the use of silica (SiO_2) bodies of OPL as a template in the synthesis of microporous carbon nanoparticles with very small particle sizes of 35-85 nm and pore sizes between 1.9 nm - 2 nm.

In modern-day scientific applications the porous nanocarbons are ubiquitous and indispensable. Porous carbon,[1] carbon nanotubes,[2] fullerenes,[3] and graphenes,[4] formed an innovative class of nanocarbons, having various applications in electronics,[5] environment,[6] energy,[7] and catalysis,[8] etc. Porous carbons can be classified according to their pore diameters as microporous (pore size<2nm), mesoporous (2nm≤pore size≤50 nm), and/or macroporous (pore size>50 nm).[9] The nanoporous carbons are fabricated by templating methods.[10] In template synthesis, the artificial silica template are formed along with carbon source. Afterward, the template is carbonized and remove the excess silica via chemical process to get porous carbon.[11] However, the template, and the carbon sources are usually two incompatible materials.[12] Hard-templating and soft-templating are the two main templating methods used in the fabrication of porous carbons, both the methods have certain limitations and drawbacks.[13] The synthesis route involves impregnation of a silica template with a carbon precursor followed by carbonization of the resulting composite and the template removal known as hard template.[14]

The silica based template are commonly used to fabricate the well-developed porous carbons because silica have natural porous structure and provide the appropriate platform for porous carbon fabrication.[14] Resorcinol formaldehyde, furfuryl alcohol, phenol, sucrose are mainly used as carbon precursors and inorganic templates include zeolites, colloidal silica, and mesoporous silica.[15] In this two-step template synthesis, the porous carbon have precise pore size and pore structure but having certain limitations such as high cost, time consuming infiltration steps, and formation of nonporous carbon on template.[16] One-step template synthesis of porous carbon carried out by carbonization of organic aerogels (supercritical CO_2)[17] and nanocomposite of carbon precursor and silica precursor followed by polymerization and carbonization steps.[18]

Herein, we describe a new carbon precursor referred as oil palm leaves (OPL) a waste lignocellulose biomass from oil palm industries which is abundant in south-east Asia. [19] OPL is consists of 47.7% holocellulose, 44.53% α-cellulose and 27.35% lignin and extractives around 20.60%.[20] We have analysed the distribution and locations of silica particles in OPL using electron microscopy (FESEM) (Figure S1 a-d) and energy dispersive X-ray (EDX). The EDX result estimate around 13.30% of silica in raw OPL (Figure S1e). The silica particles are accumulated in epidermal tissue or cell wall of leaves where transpiration induces a loss of water, which in turn increases the concentration of silica.[21] The occurrence of Si within the plant is a result of its uptake, in the form of soluble $Si(OH)_4$ or $Si(OH)_3O$-, from the soil and its controlled polymerization at a final location.[22] The individual silica bodies each consist of about 100,000 silica rods and the silica particles in each rod have a diameter of 1-2 nm.[23]

The FTIR analysis of OPL revealed the presence of Si–H bond, namely the absorption bands at 655 cm^{-1} is attributed to the stretching mode of the mono-hydrogen bond (Si–H), respectively [24] and an absorption band at 1409 cm^{-1} appears for Si-CH3 confirms the presence of Si in OPL (Figure S2a). The Si-O vibrations at 1050 cm^{-1} due to a stretching vibration where the oxygen-atom motion is in the Si-O-Si plane and is parallel to the line of two adjacent silicon atoms.[25] The XRD analysis confirms the presence of SiO_2 with different crystallite phases (110, 020, and 240) in OPL (Figure S2b). The mass degradation OPL have three different stages as showing in thermo gravimetric analysis (TGA) in Figure S2c, the OPL sample is fully degrade around 650°C and the ash the content is ~20% even after 1000 °C, because of the OPL ash having in volatile inorganic compounds mainly silica.

The transmission electron microscopy (TEM) for the carbon nanoparticles gave the regular pore image, at carbonization temperature 500 ^{o}C, where the average particle size is 80±5 nm (Figure 1a) and the pore width is 1.9-2.0 nm (Figure 2a). At 600 ^{o}C, the average particle size is 35±5 nm (Figure 1b) and the pore width also smaller compare to 500 ^{o}C with average value 1.95-1.99 nm (Figure 2a). The black spot in carbon nanoparticle are silica particles, might be presence due to incomplete removal of natural silica template. At 700 ^{o}C pyrolysis temperature the particle size is higher compare to 600 ^{o}C pyrolysis temperature and the particles are not uniformed in shape (Figure S5).

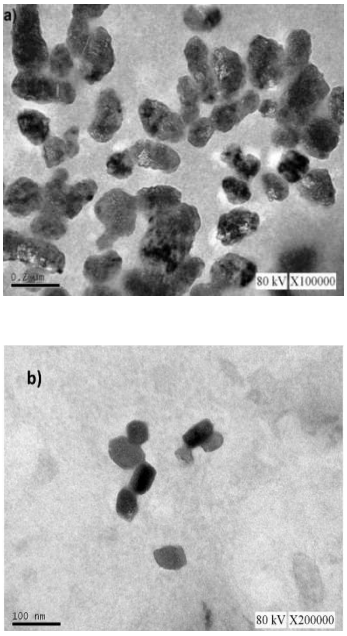

Figure 1. TEM images of PCNs with well-developed pores at (a) 500^{o}C and (b) 600^{o}C pyrolysis temperature.

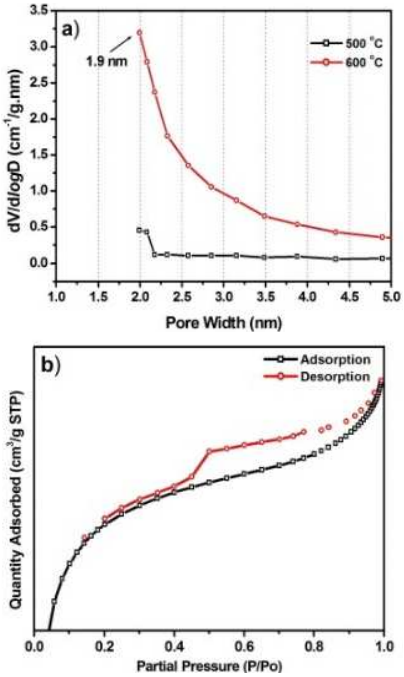

Figure 2. (a) BJH pore size distribution of PCNs at 500^{o}C and 600^{o}C pyrolysis temperature. (b) Nitrogen adsorption and desorption curve of PCNs prepared at 600^{o}C pyrolysis temperature.

FESEM images showing PNCs with average diameter around 30-40 nm with the magnification 140k for the sample pyrolysed at 600 ^{o}C as shown in Figure S3. Particle size depends on the pyrolysis temperature and 600 ^{o}C is an ideal condition to obtain uniform PCNs with low particle size. The elemental analysis results of PCNs are mentioned in Table S1, the C% at 500 ^{o}C is 78.223 % and for 600 ^{o}C is ~ 87 %. So, prepared PCNs have good carbon percentage and it increases with pyrolysis temperature.

The Brunauer-Emmett-Teller (BET) reveals that at 600 ^{o}C pyrolysis temperature the BET surface area (S_{BET}) of PCNs is 52 g.m^{-2}. The t-plot micropore surface area ($S_{t\text{-}plot}$) is equal to 39g.m^{-2}, so it indicating that the PCNs at 600 ^{o}C have very high micropore ratio 75 % ($S_{t\text{-}plot}$/ S_{BET}). This micropore percentage is higher than that the most conventional activated carbons and templated carbons.[27] The pore size of PCNs is 1.9 nm (Figure 2a, 2b). At 500 ^{o}C pyrolysis temperature the BET SBET of PCNs is 32 g.m^{-2} and St-plot is 15 g.m^{-2} (Figure 2a, S4) and the micropore percentage is ~ 47 %. So, at the higher pyrolysis temperature (at 600 ^{o}C) the surface area and the microporous carbon percentage are increases but limited to 600 ^{o}C. Due to the fact that PCNs were aggregated and intact and also exhibiting smooth surfaces, their surface area dramatically decreases as compared with earlier obtained carbon nanospheres using template method.[1]

The X-ray diffraction analysis revealed the presence of crystalline and amorphous carbon (Figure 3a). At 500 ^{o}C pyrolysis temperature, the peak at 2θ = 26.653^{o} with (002) plane for graphite (ICDD 10713739) with an interlayer d-spacing 3.3418 A^{o}. This peak may come from the low curvature graphite face found in graphite, and existing literature confirm that the peak at 26.65^{o} represent the (002) phase of graphite.[26] On the other hand at 600 ^{o}C pyrolysis temperature two peaks were observed very close together at 2θ= 26.56^{o} and 26.85^{o}, with the latter being close to the reflection for the (002) plane of graphite. At 2θ = 44.67^{o}, the (101) phase of diamond syn. (ICDD 10750410) appeared and showing the presence of (111) phase of graphite.[28] But at 500 ^{o}C this peak was not appear, may be due to the improper carbonization of precursor. The peak intensity of (002) phase shows the great difference at both the temperature, at 500 ^{o}C have lower intensity of peak, may be it contain amorphous carbon and at 600 ^{o}C higher peak intensity due to the presence of graphite carbon, this phenomenon is well documented.[29]

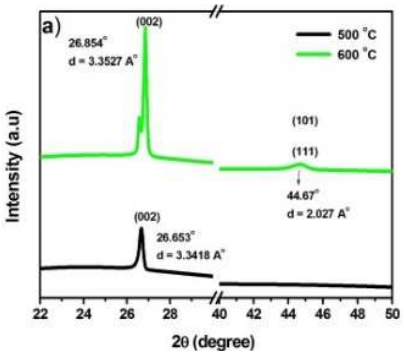

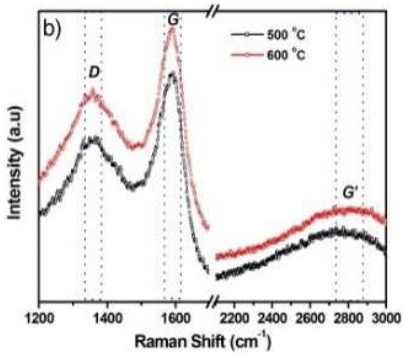

Figure 3. (a) X-ray diffraction pattern of PCNs, and (b) Raman's spectrum of porous carbon nanoparticles, showing main Raman features, the D, G and G' bands taken with a laser excitation (wavelength, 514.5 nm)) of 2.41 eV.

Raman spectroscopy is used to investigate the lattice vibrations of ordered carbon materials and extremely profound to the graphitic character of carbon structures.[30] The most prominent features in the Raman spectra of graphitic materials (Figure. 3b) are the so-called *G* band appearing in between 1580-1590 cm^{-1} (graphite), also known as a doubly degenerate phonon mode (E_{2g} symmetry) at the BZ center, is Raman active for sp^2 carbon networks. The *D* band in between 1350-1361 cm^{-1} is known as disorder-induced character of graphite. The Raman band between 2500-2800 cm^{-1} is corresponds to the overtone of *D* band is known as G'.[31] The PCNs show the *G* band at 1588 cm^{-1} and 1589 cm^{-1} for the sample pyrolysis at 600 ^oC and 500 ^oC respectively. The PCNs also possess the induced disordered, as the *D* band is present in Raman spectra (Figure 4b), at 1360 cm^{-1}, and 1358 cm^{-1} for 600 ^oC and 500 ^oC respectively. There is no much difference in the peak intensities for both *G* and *D* bands at both pyrolysis temperatures; the I_D/I_G is the integrated intensity ratio of *D* and *G* bands used for characterizing the defects quantity in graphite materials.[29] The *G* band intensity is uniform at both the pyrolysis temperature, only the *D* bands varies with temperature, so the I_D/I_G ratio is decreases from 0.73 to 0.69 at 600 ^oC compare to 500 ^oC. The G' is also present in Raman spectra for both pyrolysis temperatures, around 2800 cm^{-1}. So, it is confirm from XRD and Raman spectra, that the prepared PCNs having the high percentage of crystalline graphite.

Conclusions

In summary, a new, microporous carbon nanoparticles was synthesized using natural silica templated OPL, the cellulose, holocellulose and lignin play the role of carbon source. The carbon source is 100% from renewable lignocellulose material or waste lignocellulose material. The advantage of this carbonization process did not require any artificial silica template, catalysis, higher pyrolysis temperature, and non-renewable carbon sources. It is expected that the natural silica template with inbuilt carbon source will open a facile process to synthesize the nanoporous carbon from natural and renewable plant resources. These PCNs will provide us many application for the development and applications as advanced materials.

Acknowledgements

This work was funded by MOSTI (Ministry of Science and Technology Industry, Malaysia) for providing e-science Grant RDU130503.

Notes and references

[a] Dr. A. Kumar, Dr. G. Hegde, Ms S.A. Abdul Manaf
Faculty of Industrial Sciences & Technology,
Universiti Malaysia Pahang, Gambang 26300, Kuantan, Pahang, Malaysia.
E-mail: murthyhegde@gmail.com, hegde@ump.edu.my
[b] Dr. A. Kumar
Czech Technical University in Prague, Faculty of Civil Engineering Department of Building Structures, Thákurova 7, 166 29 Praha 6; Czech Republic.
[c] Dr. Z. Ngaini
Centre for Technology, Transfer & Consultancy (CTTC)
University Malaysia Sarawak, 94300 Kota Samarahan,
Sarawak Malaysia.
[d] Dr. K.V. Sharma
Department of Mechanical Engineering, Faculty of Engineering
University Technology PETRONAS
Bandar Seri Iskandar, 31750, Tronoh, Perak, Malaysia.

[1] A. Nieto-Marquez, R. Romero, A. Romero and J L Valverde. *J. Mater. Chem*. 2011, **21**, 1664.
[2] S. Iijma. *Nature*, 1991, **354**, 56.
[3] H W. Kroto, J R. Heath, S C. O'Brien, R F. Curl, R E. Smalley. *Nature* 1985, **318**, 162.
[4] P. Serp, R. Feurer, P. Kalck, Y. Kihn, J L. Fariam, J L. Figueiredo. *Carbon* 2001, **39**, 621–626.
[5] Z. P. Chen, W. C. Ren, L. B. Gao, B. L. Liu, S. F. Pei, H. M. Cheng. *Nat. Mater*. 2011, **10**, 424.
[6] G. P. Hao, W. C. Li, D. Qian, G. H. Wang, W. P. Zhang, T. Zhang, A. Q. Wang, F. Schuth, H. J. Bongard, A. H. Lu. *J. Am. Chem. Soc*. 2011, **133**, 11378.
[7] Z. S. Wu, Y. Sun, Y. Z. Tan, S. Yang, X. Feng, K. Müllen. *J. Am. Chem. Soc*. 2012, **134**, 19532.
[8] a) P. Zhang, Y. Gong, H. Li, Z. Chen, Y. Wang. *Nat. Commun*. 2013, **4**, 1593; b) T. P. Fellinger, F. Hasché, P. Strasser, M. Antonietti. *J. Am. Chem. Soc*. 2012, **134**, 4072.
[9] J. Rouquerol, D. Avnir, C. W. Fairbridge, D. H. Everett, J. H. Haynes, N. Pernicone, J. D. F. Ramsay, K. S. W. Sing, K. K. Unger. *Pure & Appl. Chem*. 1994, **66(8)**, 1739.
[10] a) Y. Fang, Y. Y. Lv, R. C. Che, H. Y. Wu, X. H. Zhang, D. Gu, G. F. Zheng, D. Y Zhao. *J. Am. Chem. Soc*. 2013, **135**, 1524; b) H. L. Jiang, B. Liu, Y. Q. Lan, K. Kuratani, T. Akita, H. Shioyama, F. Zong, Q. Xu. *J. Am. Chem. Soc*. 2011, **133**, 11854; c) Y. S. Hu, P. Adelhelm, B. M. Smarsly, S. Hore, M. Antonietti. Maier. *J. Adv. Funct. Mater*. 2007, **17**, 1873; d) J. Shinae, H. J. Sang, R. Ryong, K. Michal, J. Mietek, L. Zheng, O. Tetsu, T. Osamu. *J. Am. Chem. Soc*. 2000, **122**, 10712.

[11] A. U. Lu, T. Sun, W. C. Li, Q. Sun, D. H. Liu, Y. Guo. Angew. *Chem. Int. Ed*. 2011, **50**, 11765.
[12] L. Zhenghui, W. Dingcai, L. Yeru, F. Ruowen, M. Krzysztof. *J. Am. Chem. Soc*. 2014, **136**, 4805.
[13] a) D. Wu, H. Dong, J. Pietrasik, E. K. Kim, C. M. Hui, M. Zhong, M. Jaroniec, T. Kowalewski, K. Matyjaszewski. Chem. Mater. 2011, 23, 2024; b) Y. R. Liang, R. W. Fu, D. C. Wu. ACS Nano. 2013,7, 1748; c) B. H. Han, W. Zhou, A. Sayari. *J. Am. Chem. Soc*. 2003, **125**, 3444.
[14] a) R. Ryoo, S. H. Joo, S. Jun. J. Phys. Chem. B. 1999, 103(37), 7743; b) K. P. Gierszal, M. Jaroniec. J. Am. Chem. Soc. 2006, 128, 10026; c) K. P. Gierszal, M. Jaroniec. J. Phys. Chem. C 2007, 111, 9742; d) M. Jaroniec, J. Choma, J. Gorka, A. Zawislak. *Chem. Mater*. 2008, **20**, 1069.
[15] a) S. H. Joo, S. J. Choi, I. Oh, J. Kwak, Z. Liu, O. Terasaki, R. Ryoo. Nature, 2001, 412, 169; b) R. Ryoo, S. H. Joo, M. Kruk, M. Jaroniec. *Adv. Mater*. 2001, **13**, 677.
[16] G. P. Meisner, Q. Hu. *Nanotech*. 2009, **20**, 204023.
[17] a) H. Tamon, H. Ishizaka, M. Mikami, M. Okazaki. Carbon. 1997, 35, 791; b) J. Ozaki, N. Endo, W. Ohizumi, K. Igarashi, M. Nakahara, A. Oya, S. Yoshida, T. Iizuka. Carbon. 1997, 35, 1031; c) S. Gavalda, K. E. Gubbins, Y. Hanzawa, K. K. Kaneko, T. Thomson. *Langmuir*, 2002, **18**, 2141.
[18] a) B-H. Han, W. Zhou, A. Sayari. J. Am. Chem. Soc. 2003, 125, 3444; b) Q. Hu, J. Pang, N. Jiang, J. E. Hampsey, Y. Lu. *Microporous Mesoporous Mater*. 2005, **81**, 149.
[19] a) O. Chavalparit, W. H. Rulkens, A. P. J. Mol, S. Khaodhair. Environ. Develop & Sust. 2006, 8, 271; b) M. Rafatullah, T. Ahmad, A. Ghazali, O. Sulaiman, M. Danish, M. Hashim. *Crit. Rev. in Environ. Sci. and Tech*. 2013, **43(11)**, 1117.
[20] R. Hashim, W. N. A. W. Nadhari, O. Sulaiman, F. Kawamura, S. Hiziroglu, M. Sato, T. Sugimoto, T. G. Seng, R. Tanaka. *Mater. Des*. 2011, **32**, 246.
[21] a) H. A. Currie, C. C. Perry. Ann. Bot. 2007, 100, 1383; b) E. Blackman. *Ann. Bot*. 1968, **32**, 207.
[22] a) N. Mitani, J. F. Ma. J. Exp. Bot. 2005, 56, 1255; b) C. J. Prychid, P. J. Rudall, M. Gregory. Bot. Rev. 2003, 69, 377; c) L. Jones, K. Handreck. *Agron*. 1967, **19**, 107.
[23] P. Dayanandan. *Scan. Electron Microscop*. 1983, **3**, 1519.
[24] a) J. C. Knights, G. Lucovsky, R. J Nemanich. *J. Non-Crys. Solids*. 1979, **32**, 393; b) L. Gao, N. P. Lu, L. G. Liao, A. L. Ji, Z. X. Cao. *J. Phys. D: Appl. Phys*. 2012, **45**, 335104.
[25] a) F. L. Galeener. *Phys. Rev. B* 1979, **19**, 4249; b) F. L. Galeener, P. N. Sen. *Phys. Rev. B* 1978, **17**, 1928; c) L. Gao, N. P. Lu, L. G. Liao, A. L. Ji, Z. X. Cao. *J. Phys. D: Appl. Phys*. 2012, **45**, 335104.
[26] Z. H. Li, D. C. Wu, Y. R. Linag, F. Xu, R. W. Fu. *Nanoscale* 2013, **5**, 10824.
[27] a) C. W. Wang, W Yuan, J. Graser, R. Zhao, F. Gao, M. J. O'Connell. *ACS Nano*. 2013, **7(12)**, 11156; b) Y-H. Lin, Y-C. Chi, G-R. Lin. *Laser Phys. Lett*. 2013, **10**, 055105.
[28] J-T. Wang, C. Chen, E. Wang, Y. Kawazoe. *Scienti. Repor*. 2014, **4**, 4339.
[29] P. L. Jr. Walker, J. F. Rakszawski, A. F. Amington. ASTM Bulletin No. 208. 1955.
[30] J. P. Tessonnier, D. Rosenthal, T. W. Hansen, C. Hess, M. E. Schuster, R. Blume, F. Girgsdies, N. Pfänder, O. Timpe, D. S. Su, R. Schlögl. *Carbon*. 2009, **47**, 1779.
[31] a) P. Lespade, R. Al-Jishi, M. S. Dresselhaus. *Carbon*. 1982, **20**, 427; b) L. G. Cançado, M. A. Pimenta, R. A. Neves, G. Medeiros-Ribeiro, T. Enoki, Y. Kobayashi, K. Takai, K. Fukui, M. S. Dresselhaus, R. Saito, A. Jorio. *Phys. Rev. Lett*., 2004, **93**, 047403; c) F. Tuinstra, J. L. Koenig. *J. Phys. Chem*., 1970, **53**, 1126.